JOURNAL OF PROPULSION AND POWER
Vol. 19, No. 4, July–August 2003

Theoretical Performance of a Magnetohydrodynamic-Bypass Scramjet Engine with Nonequilibrium Ionization

Chul Park* and David W. Bogdanoff†
ELORET Corporation, Sunnyvale, California 94087
and
Unmeel B. Mehta‡
NASA Ames Research Center, Moffett Field, California 94035

The theoretical performance of a scramjet propulsion system in which a magnetohydrodynamic (MHD) energy bypass scheme is operated in a nonequilibrium ionization environment is evaluated. In the MHD generator, the incoming airflow at a temperature too low to produce the required ionization is seeded with cesium and ionized by the use of an unspecified external power source. The resulting nonequilibrium environment is described using a two-temperature model. The accelerator is operated with equilibrium ionization. The expansion through the nozzle is calculated with account taken of finite rate reactions, and the boundary layer is assumed to be fully turbulent. The results show that the required external power is of the same order of magnitude as that of the power generated in the MHD generator. An MHD energy bypass propulsion scheme looks to be more promising with the equilibrium ionization method than with the nonequilibrium ionization method.

Nomenclature

A = cross-sectional area of flow path, m^2
B = magnetic field strength, T
E_e = vibron (vibrational-electron) energy, J/kg, Eq. (1)
$E_{e,r}$ = E_e evaluated at $T_{e,r}$, J/kg
E_x = axial voltage gradient, V/m
E_y = transverse electrical field strength, V/m
H = static enthalpy excluding E_e, J/kg
I_{sp} = specific impulse for $h_4 = 1$, s
I_{sp_x} = specific impulse for $h_4 \neq 1$, Eq. (12), s
j = electrical current density, A/m^2
M = Mach number
M_c = combustor entrance Mach number
P = external ionizing power, W
p = pressure, Pa
q = density of external ionizing power, W/m^3
R_1 = electron-heavy particle energy transfer rate, Eq. (8), W/kg
R_2 = vibration-heavy particle energy transfer rate, Eq. (8), W/kg
T = gas (heavy particle) temperature, K
T_e = vibron (vibrational-electron) temperature, K
$T_{e,r}$ = T_e required for magnetohydrodynamic generator, K
t = time, s
u = axial velocity, m/s
V = flight velocity, m/s
x = axial distance, m
x_{eq} = equilibration distance, m
y = transverse (normal to B and u) distance, m
γ_i = concentration of species i, mol/kg
η_1 = external-to-combustor power ratio
η_2 = external-to-generator output power ratio
η_3 = energy bypass ratio
η_4 = fuel-to-external power conversion efficiency
θ = ramp angle, deg
ρ = density, kg/m^3
σ = electrical conductivity, mho/m

Received 29 January 2001; revision received 10 July 2001; accepted for publication 15 March 2003.

*Senior Research Scientist, Mail Stop 230-2, NASA Ames Research Center, Moffett Field, CA 94035; cpark@mail.arc.nasa.gov. Fellow AIAA.
†Senior Research Scientist, Mail Stop 230-2, NASA Ames Research Center, Moffett Field, CA 94035; dbogdanoff@mail.arc.nasa.gov. Associate Fellow AIAA.
‡Division Scientist, Space Technology Division, Mail Stop 229-3, NASA Ames Research Center, Moffett Field, CA 94035; Unmeel.B.Mehta@nasa.gov. Associate Fellow AIAA.

Introduction

In a recently proposed concept,[1] the performance of a scramjet propulsion system is improved by the use of a magnetohydrodynamic (MHD)-energy bypass scheme. In this scheme, an MHD generator, in the course of generating electrical power, decelerates the flow entering the combustor, thereby providing a greater time to complete supersonic combustion. The electrical power generated in the process is used in an MHD accelerator positioned after the combustor to accelerate the flow before expanding through the nozzle.

To apply MHD to a flow, the flow must be electrically conductive. This can be achieved by seeding the flow with either potassium or cesium. Even with seeding, the flow must be sufficiently hot to ionize the seed species; typically, 3000 K is needed. In the accelerator, which accepts the flow emerging from the combustor, the flow is usually sufficiently hot for ionization. However, in the generator, which accepts the flow emerging from the inlet compression process, the flow is not necessarily sufficiently hot.

In the theoretical studies made in Refs. 2 and 3 in which the performance of MHD-energy bypass propulsion systems is analyzed theoretically, ionization is achieved in both the generator and the accelerator in a thermochemical equilibrium environment. Liquid hydrogen is the fuel for the system. Ionization in the generator is achieved by the shock compression of the oncoming airflow. In this equilibrium scheme, the static pressure reaches a few atmospheres in both generator and accelerator. The calculations[2,3] show that the MHD bypass scheme offers a possibility of improvement of the scramjet performance in a certain range of flight speeds. The performance gain in this scheme is limited by the strong compression needed to produce ionization also producing a large drag.

There is also a concept, in which the MHD generator is operated in a thermochemical nonequilibrium regime.[4] In this concept, the MHD generator will be operated in a low-temperature, low-pressure environment. Ionization is produced by the application of external power, for example, with an electric discharge. The advantage of

such a scheme is that a much weaker shock compression is needed upstream of the generator, which would produce considerably less drag.

In Ref. 5, we estimated the overall performance of a scramjet system operating on such a nonequilibrium ionization principle. Flowpath calculations were performed for five different MHD-energy bypass system configurations, one producing two shock waves and four producing four shock waves. The nonequilibrium environment in the generator was analyzed using a two-temperature model.[6] Comparisons are made of the specific impulse values with those of a conventional scramjet without MHD bypass.

However, two small errors of a numerical nature were found in Refs. 2, 3, 5: 1) The enthalpy values calculated by the equilibrium subroutine used was mistakenly considered to be referenced to 0 K, whereas, in fact, it was referenced to 298 K. 2) The sound speed was calculated imprecisely. These errors are corrected herein. Because the present results are at least qualitatively the same as those in Ref. 5, some results, those considered nonessential in the flow of logic, are not shown in the present work. Readers are referred to Ref. 5 for those missing details.

Method

Density Regime

Operating an MHD generator with nonequilibrium ionization implies that the flow density is low therein. The simplest scramjet system operating on the nonequilibrium MHD principle is one that produces two oblique shock waves of equal turning angles, one over a ramp and the other on the cowl that forms a second ramp. The MHD generator is placed after these two shocks. The density over the first ramp is lower than that over the second ramp, but it would not be practical to place the MHD generator over the first ramp because doing so would produce a nonuniform flow.

The density level in the MHD generator in such a system is determined by the ramp angle, flight dynamic pressure, and flight velocity. The dynamic pressure will be assumed to be 1 atm in most of the present work. The flight velocity V will be varied from 2500 to 4000 m/s. There is a practical lower limit to the ramp angle; below the limit, it is not possible to construct a viable airframe structure. In the present study, the lower limit will be considered to be 5 deg. This choice of dynamic pressure, flight velocity, and ramp angle leads to a minimum density, pressure, temperature, and total number density achievable in the MHD generator: 7.0×10^{-2} kg/m^3, 1.4×10^4 Pa (0.14 atm), 715 K, and 1.5×10^{24} m^{-3}, respectively. The temperature is too low to produce the equilibrium ionization level needed for MHD action.

Ionization Schemes

In both equilibrium and nonequilibrium schemes, ionization can be facilitated when the flow is seeded with an alkali metal such as potassium or cesium. In Refs. 2 and 3, it is concluded that potassium and cesium are approximately equally effective in an MHD bypass scheme based on the equilibrium principle. In the present work, cesium in atomic form is assumed to be uniformly injected at the entrance of the MHD generator. In Refs. 2 and 3, the ionization fraction attained was in the order of 10^{-4}. The same level of ionization will be assumed in the present work. Because the lowest number density under consideration is 1.5×10^{24} m^{-3}, the lowest electron density to be considered is about 10^{20} m^{-3}.

Cesium can be ionized, in a nonequilibrium condition, by several means. The first possible scheme is a high-voltage electrical discharge. In air containing a small concentration of cesium, an electric discharge will first ionize nitrogen and oxygen molecules, producing N_2^+ and O_2^+. These ions will transfer their ionization to cesium through charge-exchange collisions. Because the ionization energies of the molecules are approximately three times that of cesium, the process will triple the degree of ionization. The end result is the ionization of cesium. A second possible scheme is ultraviolet irradiation. Cesium atoms can be ionized by irradiation of wavelengths shorter than 319 nm, which can be provided by a xenon lamp. In this case, the applied energy is expended directly to ionize and heat electrons. In both of these schemes, the nonequilibrium state produced can be characterized relatively easily. Electron beam[4] and alpha particles[7] may also be used to produce nonequilibrium ionization. However, the characteristics of the nonequilibrium state produced by these schemes are less certain.

In the equilibrium region, the equilibrium state is calculated with the well-known JANNAF coefficients.[8] JANNAF coefficients are used here even though they are known to be less accurate at low temperatures than the also well-known McBride coefficients,[9] because the latter is found to yield faulty degrees of ionization in the regime of temperature of interest. The inaccuracy of the JANNAF coefficients at low temperatures produces a small inaccuracy, as will be discussed in the "Discussion" section.

Two-Temperature Phenomenon

At the electron density of 10^{20} m^{-3} under consideration, collisions between the electrons produced by the aforementioned methods and cesium ions and atoms will be sufficiently fast to bring the ionization phenomenon to equilibrium within a short time. That is, the electron density and temperature will adjust themselves to satisfy the well-known Saha equation, though the electron temperature may be very different from the gas (heavy-particle translational) temperature. This forces the electron temperature of consideration to be between about 2500 and 3500 K. The production of higher electron temperatures and densities would require an unnecessary expenditure of power.

It is well known that the interaction between electrons and the vibrational mode of nitrogen molecules is very fast.[10] At the electron temperature of 3000 K and total number density of 1.4×10^{24} m^{-3}, the vibrational temperature of N_2 and the electron temperature equalize within about 10^{-7} s. The vibrational temperature of O_2 molecules will approach the vibrational temperature of N_2 because of the so-called vibration-to-vibration interaction, though at a slower rate.[6]

By assuming that the vibrational temperatures of N_2 and O_2 are the same as the electron temperature, one arrives at the well-known two-temperature model.[6] For later reference, this common temperature will be called the vibron temperature and designated T_e. The energy associated with this temperature will be called the vibron energy, and designated E_e. This is equal to the energy of ionization of cesium, plus the kinetic energy of electrons, plus the vibrational energy of N_2 and O_2. (It will be shown later that the last component, the vibrational energy, is by far the largest of the three.)

The static enthalpy of the flow can then be broken into two parts: 1) E_e and 2) H, which contains the translational, rotational, and the electronic excitation energies of the heavy particles. The electronic excitation energy is very small in the temperature regime of consideration and, therefore, its combination with translational and rotational energies, though unusual, is inconsequential.

In some of the ionization schemes, the external power may be applied in a pulse form, either temporally or spatially. As long as the rate of such pulses is sufficiently fast to form a meaningful average over a timescale or dimension scale of practical interest, for example, over 1 ms or 1 cm, then the two-temperature approximation will be valid.

An exception to the present argument will occur when the ionization scheme produces electrons of very high temperature. When the electron temperature is very high, the collision cross sections between electrons and ions and between electrons and the vibrational mode of N_2 become very small. Therefore, the two-temperature environment will evolve much more slowly. This condition is known as the runaway condition. Little is known about the MHD action in such an environment. Therefore, such an environment is excluded from consideration.

Conservation Equations

As was done in Refs. 2 and 3, an ideal one-dimensional flow with Faraday-type MHD devices (i.e., with the electrical current flowing in the direction perpendicular to the direction of flow) will be assumed. A power density q is assumed to be expended to produce the required ionization.

To operate an MHD generator in a nonequilibrium regime, E_e at the entrance of the generator $E_{e,0}$, which is low, must be raised to a required level $E_{e,r}$. This can be achieved, for example, by letting the airflow pass through a curtain of ultraviolet radiation. The power required to do so is

$$P_0 = \rho u A(E_{e,r} - E_0) \tag{1}$$

The power density q required to deposit P_0 into the vibron mode is obtained by dividing P_0 by AD_x, where D_x is the distance over which this q value is maintained. It is assumed that D_x is infinitesimally small. That is, P_0 is applied impulsively.

After the required vibron energy $E_{e,r}$ is achieved, finite external power must still be applied to keep E_e at that level. Otherwise, the collisions between the vibron group and the molecules at a lower temperature will lower the vibron energy. The external power required to keep E_e at $E_{e,r}$ can be determined from the conservation relations, which include the following:

Species mass

$$\rho u \frac{\mathrm{d}\gamma}{\mathrm{d}x} = \rho \frac{\partial \gamma}{\partial t} \tag{2}$$

global mass

$$\rho u A = \text{const} \tag{3}$$

momentum

$$\rho u \frac{\mathrm{d}u}{\mathrm{d}x} = -\frac{\mathrm{d}p}{\mathrm{d}x} + jB \tag{4}$$

total energy

$$\rho u \frac{\mathrm{d}}{\mathrm{d}x}\left(H + E_e + \frac{u^2}{2}\right) = \frac{j^2}{\sigma} + uBj + q \tag{5}$$

and vibron energy

$$\rho u \frac{\mathrm{d}E_e}{\mathrm{d}x} = \frac{j^2}{\sigma} - \rho \frac{\partial E_e}{\partial t} + q \tag{6}$$

The quantity $\partial\gamma/\partial t$ in Eq. (2) is the rate of chemical reaction for species i. The expression for this rate can be found, for example, in Ref. 10. We have used the relation $j = \sigma(E - uB)$ to obtain the form of Eq. (5) shown. The quantity $\partial E_e/\partial t$ in Eq. (6) is the rate of energy transfer from the vibron mode to the translational–rotational mode. It has two components: $\partial E_e/\partial t$ is the collisional energy transfer rate, which equals the electron–heavy particle energy transfer rate, plus the vibration–translation energy transfer rate, which equals $R_1 + R_2$. $R_1 + R_2$ is positive when $T_e > T$. The expressions for the two components can be derived with the information in Ref. 6.

To operate an MHD device, E_e must be kept nearly constant. By the requirement that E_e be constant, the left-hand side of Eq. (6) is set to zero, leading to

$$q = \rho \frac{\partial E_e}{\partial t} - \frac{j^2}{\sigma} \tag{7}$$

The total energy equation (5) becomes

$$\rho u \frac{\mathrm{d}}{\mathrm{d}x}\left(H + \frac{u^2}{2}\right) = \rho \frac{\partial E_e}{\partial t} + uBj \tag{8}$$

There exist two constraints to this system of equations, that is, on load factor E_y/uB and the allowed axial voltage gradient E_x (Refs. 2 and 3). These two constraints specify the magnetic field strength B and the electrical current density j.

For a specified cross-sectional area distribution, one can determine all properties in the nonequilibrium region by solving Eqs. (2–4), (7), and (8) simultaneously, under the last two constraints. By adding P_0 [Eq. (1)] to the integration of q over the volume, one obtains the external power required P:

$$P = P_0 + \int q A \, \mathrm{d}x \tag{9}$$

Performance Calculation

The performance of the overall system is calculated in the same manner as in Refs. 2 and 3, except for the nonequilibrium region in the MHD generator just discussed. In addition to the configuration mentioned earlier, which produces two oblique shock waves, four configurations producing four shock waves are considered. The five configurations studied are shown schematically in Figs. 1a–1e. The two-shock configuration in Fig. 1a is identified as configuration 0. The four shock configurations, 1–4, are considered because they generally produce lower Mach numbers and higher pressures at the entrance of the combustor than the two-shock scheme. In configurations 1 and 2, the flow exiting from the MHD generator undergoes two more shock compressions. In configurations 3 and 4, the two additional shock compressions occur before entering the generator. In configurations 1 and 3, the third and fourth shocks occur in the yaw plane. Such a two-plane four-shock compression system was considered in Ref. 3. In configurations 2 and 4, the third and fourth shocks occur in the pitch plane. Such a single-plane four-shock compression system was considered in Ref. 2.

There are four ratios that are associated with the performance of the nonequilibrium MHD scheme: 1) the ratio of the external power P to the power of the fuel consumed in the combustion chamber η_1; 2) the ratio between the external power P and the power output from the MHD generator (the integral of the product of electrical current and voltage over the flow volume in the generator) η_2; 3) the energy bypass ratio, which is the ratio between the electrical power output by the MHD generator to the flow power $\rho u A(H + u^2/2)$ at the entrance of the generator η_3; and 4) the ratio of the external power to the power of the fuel expended to produce the external power, for example, by a hydrogen–oxygen fuel cell, η_4.

In the calculation of η_4, the fuel energy expended in the device, for example, the fuel cell, is calculated under the assumption that molecular hydrogen is converted completely to form water vapor. The temperature of the combustion product is brought to the room temperature, 298 K, which gives 119.9 MJ/kg. The fuel flow rate consumed to produce the external power is then $P/(1.199 \times 10^8 \eta_4)$. The specific impulse for $\eta_4 = 1$ will be designated I_{sp}. The calculation results will be presented in terms of this quantity. For cases $\eta_4 \neq 1$, the specific impulse, I_{sp_x}, is calculable by

$$I_{\mathrm{sp}_x} = I_{\mathrm{sp}} \frac{1 + \eta_1}{1 + \eta_1/\eta_4} \tag{10}$$

Assumptions and Parameters

The assumptions stated, and other parameters not specified, are summarized here.

Vehicle

1) The flight dynamic pressure is taken to be 1 atm for most of the calculations. Two other values, 0.5 and 2 atm, will be considered toward the end of the work.

2) The width of the vehicle is infinite. However, all performance values, such as thrust, are given per 1 m of width. For configurations 1 and 3, each engine units is typically 2–3 m wide. The performance values for each unit are divided by the width of the unit to obtain the per meter value. The length of the vehicle is chosen arbitrarily to be 46 m. The lengths of the MHD generator, combustor, and MHD accelerator are equal to or less than 2.72, 0.48, and 2.84 m, respectively. For the four-shock system, the ramp angle for the third shock is the same as that for the first shock. For configurations 1 (Fig. 1b) and 3 (Fig. 1d), the cross section of the combustor is a square. All of these parameters are the same as those used in Refs. 2 and 3. The nozzle geometry is also that given in Refs. 2 and 3.

3) The length of the first ramp is 30 m for the two-shock configuration (Fig. 1a), 20 m for configurations 1–3, and 10 m for configuration 4. These lengths result in approximately the same length nozzle. However, there are small differences in the height of the vehicle and, therefore, in the airflow rate captured.

4) The fuel equivalence ratio is 1. Fuel is uniformly mixed with air, and equilibrium is reached within the combustor.

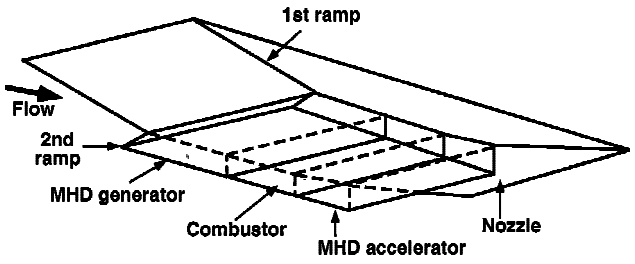

a) Two-shock design, configuration 0

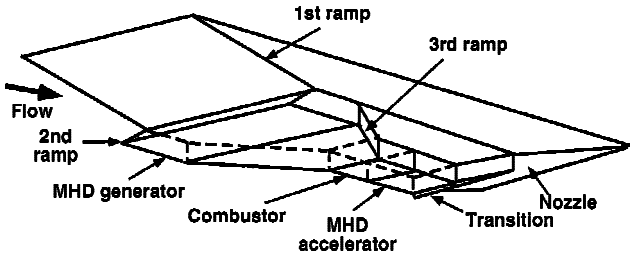

b) Four-shock design, configuration 1

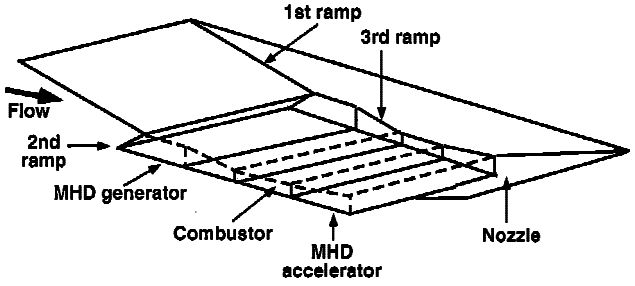

c) Four-shock design, configuration 2

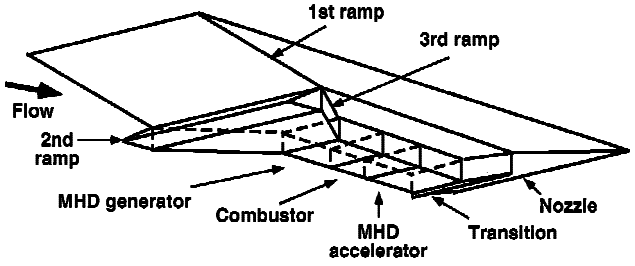

d) Four-shock design, configuration 3

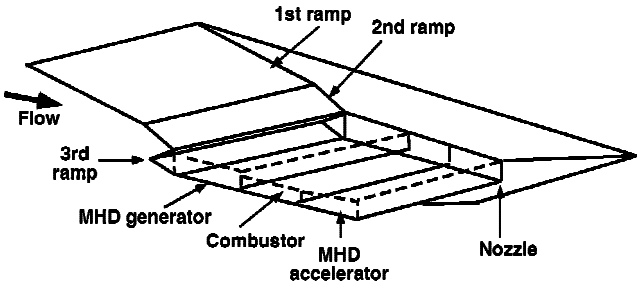

e) Four-shock design, configuration 4

Fig. 1 Perspective view of the designs considered.

5) The ratio between the exit cross section and the entrance cross section of the combustor, which is usually slightly larger than unity to prevent choking, is kept to the lowest nonchoking value.

6) The boundary layer is fully turbulent, starting from the nose tip. Turbulent skin friction in the flowpath is calculated by the use of the method of Ref. 11. The thrust of the system is calculated in the present work as the inviscid thrust minus the skin-friction drag in the flowpath.

7) The heat transfer phenomenon and multidimensional flow phenomena such as separation are neglected.

8) Calculations are made at ramp angle intervals of 0.1 deg to determine the maximum specific impulse.

MHD Devices

1) The load factor E_y/uB is taken to be 0.95 for the generator and 1/0.95 for the accelerator for most of the calculations. The E_y and u are those in the inviscid region. The pairs (0.9, 1/0.9), (0.85, 1/0.85), and (0.8, 1/0.8) are considered toward the end of the work.

2) Both the generator and the accelerator are considered to be Faraday devices (electrical current in the direction normal to the flow direction).

3) The cross-sectional area A in Eq. (3) is constant in the nonequilibrium region of the MHD generator.

4) The seed material is cesium in an atomic form. Its mass fraction with respect to air is 3×10^{-3}. This means that the mass of the seed material needed is 10.3% of that of fuel. Seeding is instantaneous, and no energy is expended in seeding.

5) The required vibron temperature for configurations 0–2 is $T_{e,r} = 2800$ K. For configurations 3 and 4, $T_{e,r} = 3200$ K is used because the gas density in the generator is higher for these configurations. These result in an electrical conductivity between 40 and 110 mho/m, depending on flight velocity and ramp angle.

6) The maximum allowed axial voltage gradient E_x is about 5000 V/m. This value was assumed in Refs. 2 and 3.

Results

Nonequilibrium Behavior

In Fig. 2, the behavior of the gas temperature T and the external power density q are shown for the case where the flight velocity V and ramp angle θ are 3500 m/s and 6 deg, respectively. The gas temperature in the generator T approaches T_e and eventually reaches a plateau. One can define the equilibration distance x_{eq} as the distance at which the difference between T_e and T is 10% of its value at the entrance, $(T_e - T)/(T_e - T)_{entrance} = 0.1$. At the point where dT/dx is 10 K/m, the nonequilibrium calculation is terminated, and the equilibrium calculation[2,3] is started. There is a small discontinuity in T and T_e at the switchover point. However, this discontinuity is believed to be inconsequential.

The initial impulsive external power needed for ionization, Eq. (1), is 102 MW for this case, as indicated in Fig. 2. The total external power to the point where the nonequilibrium analysis is finished, given by Eq. (9), is 464 MW, also indicated in Fig. 2. The difference, 362 MW, is expended in preventing the vibron temperature T_e from falling to the gas temperature T. The electron density generated by the external power, and held approximately constant thereafter, is 1.5×10^{20} m^{-3}, which results in electrical conductivity of 105 mho/m. Of the vibron energy, 99.5% consists of the vibrational energy. The external energy expended $E_{e,r}$ is 58% of the static enthalpy and about 7% of the total enthalpy of the flow. Cooling of

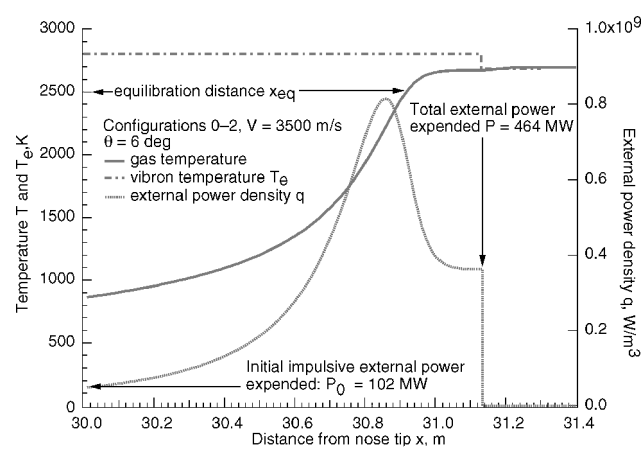

Fig. 2 Typical variation of gas temperature and the required external power in an MHD generator after two shocks: $V = 3500$ m/s and $\theta = 6$ deg.

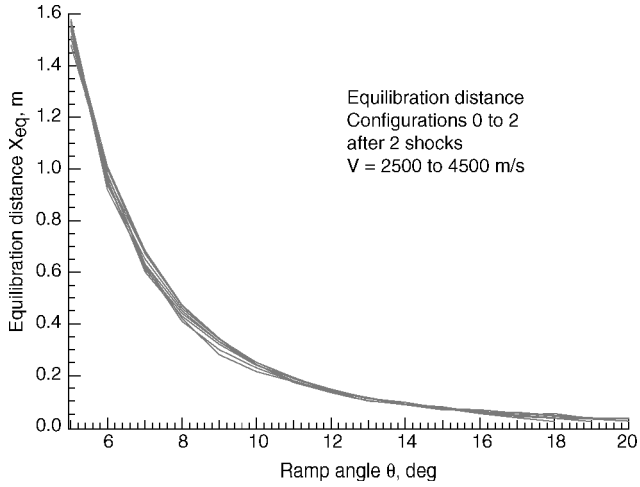

Fig. 3 Equilibration distance in the MHD generator after two shocks.

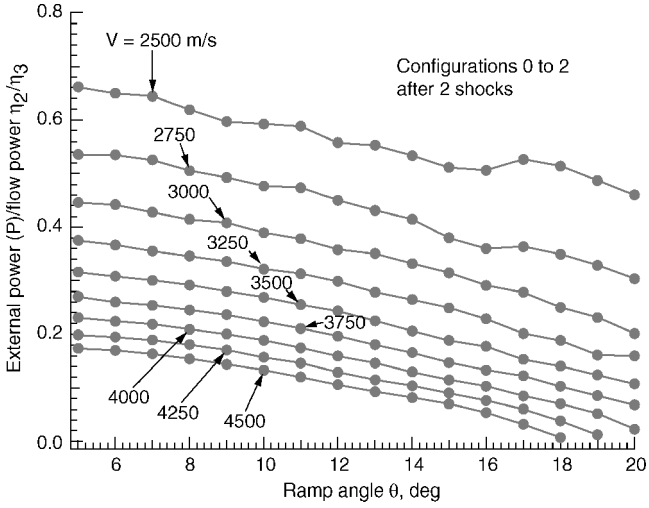

Fig. 4 External power required P divided by flow power $\rho uA(H + u^2/2)$.

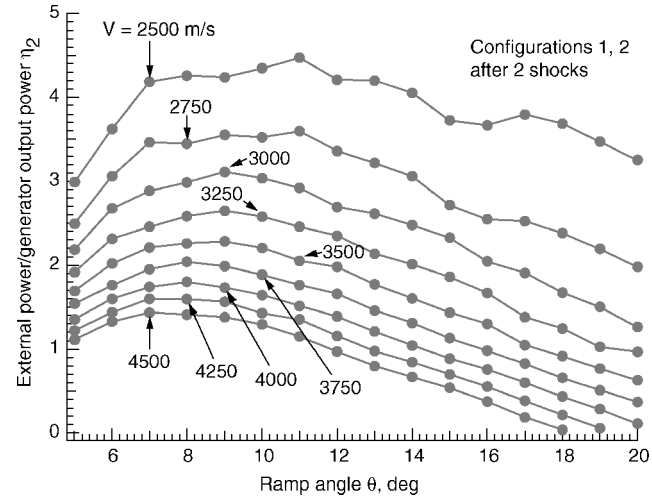

a)

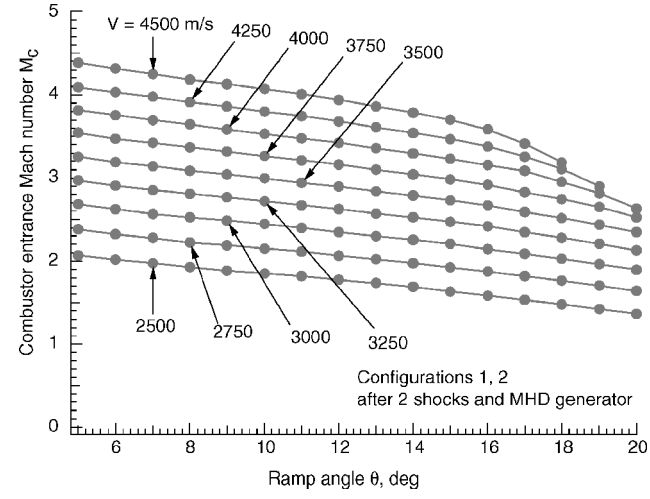

b)

Fig. 5 Parameters of configurations 1 and 2, with a) ratio of the external power to the generator output power and b) Mach number.

the vibron energy is almost entirely (98.6%) by the vibron–heavy particle translation energy transfer phenomenon R_2. Immediately after the application of P_0, the first term comprises about 90% of the sum of the two terms in the expression for q in Eq. (7).

When T equilibrates with T_e, the entire flow is heated to a temperature slightly below the prescribed T_e of 2800 K. Thus, the effect of application of the external power is to heat the entire gas mass to approximately T_e. This makes the application of external power an expensive measure. If potassium is used instead of cesium, the required T_e and, consequently, the required external power, will be higher. If the flow is not seeded, the required T_e and external power will be higher still.

In Fig. 3, the equilibration distance is shown as a function of flight velocity V and ramp angle θ. As seen here, the relaxation distance is less than 1.6 m for all cases.

External Power Required

The external power required, normalized by the flow power $\rho uA(H + u^2/2)$, for configurations 0–2 is shown in Fig. 4. From the definition of η_2 and η_3, the ratio shown in Fig. 4 becomes η_2/η_3. As Fig. 4 shows, the external power is a significant fraction of the flow power.

For configurations 1 and 2, the ratio of the external power P to the generator output power and the combustor entrance Mach number M_c are calculated as a function of V and θ and are, respectively, plotted in Figs. 5a and 5b. The upper limit in θ in Figs. 5a and 5b for each V value is set by either of the following: 1) The gas temperature after the first two shocks is greater than the temperature required for ionization ($T_{e,r} = 2800$ K). 2) the Mach number after the third shock is too small to support an oblique fourth shock.

As Fig. 5a shows, in most cases, the external power is larger than the output from the generator ($\eta_2 > 1$). When η_2 is less than unity, which occurs at high ramp angles and high flight velocities, the MHD process can be self-sustaining by diversion to and expenditure of a portion of the generator output as the external power. For example, for $V = 3750$ m/s and $\theta = 19$ deg, 56% of the generator output can be expended to provide the needed external power, and the remainder, 44%, can be expended for acceleration. The power required is higher at low speeds, as expected. The power approaches zero as θ increases. This is also expected: As θ increases, the gas temperature after two shocks becomes high, and only a small amount of energy is needed to raise the gas temperature to that required for MHD action.

According to Fig. 5b, the combustor entrance Mach number M_c is low at low V and high θ, which is expected. At the highest θ and the lowest velocity values calculated, M_c decreases toward unity. The present calculation procedure does not allow subsonic flow. However, Fig. 5 suggests that M_c could be made subsonic by the present method. In such a case, precautions would have to be taken to avoid choking the flow and unstarting the engine.

Specific Impulse

As mentioned in the "Introduction," the main purpose of consideration of MHD schemes for a scramjet system is to lower the flow Mach number at the entrance of the combustor M_c and to improve the performance of the scramjet system. The flowpath calculations

are made with the five configurations shown in Figs. 1a–1e at different flight velocities while M_c is constrained to be less than either 1.5, 2.0, or 2.5. The ramp angle θ giving the highest viscous specific impulse is the optimum angle for that particular design and flight velocity. According to this procedure, M_c varies from a low supersonic value at low velocities to the allowed maximum value at high velocities. In Figs. 6a–6c, the specific impulse values for the optimum conditions are compared. The specific impulse of 450 s for the space shuttle main engine (SSME) is also shown for comparison.

According to Figs. 6a–6c, at low speeds and $M_c > 1.5$, configurations 3 and 4 give higher specific impulses. These configurations lead to equilibrium ionization at high speeds, and, therefore, the nonequililbrium scheme does not function there, as mentioned earlier. Of these two, configuration 4 is better. At higher velocities, only configurations 1 and 2 function as a nonequilibrium device. Of these, configuration 1 gives a higher specific impulse.

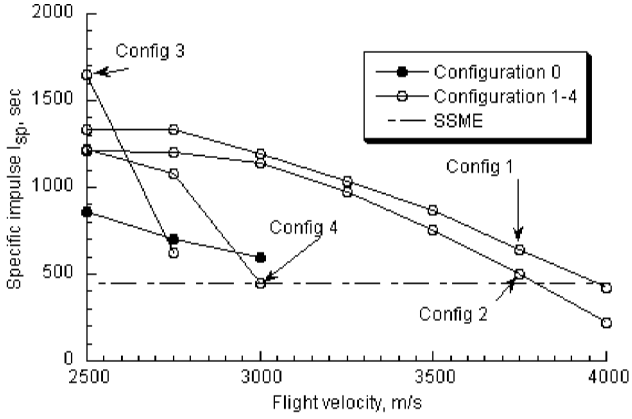

a) Combustor entrance Mach number M_c less than 1.5

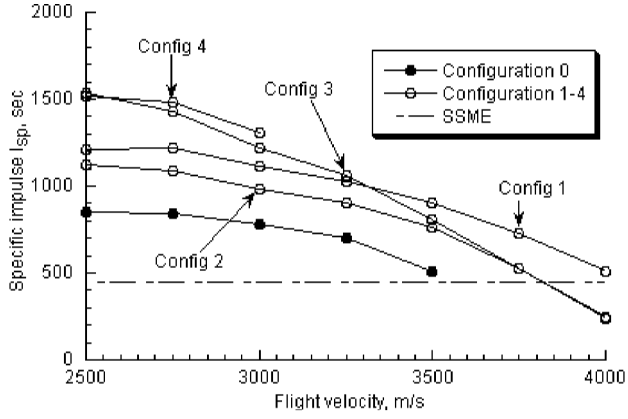

b) Combustor entrance Mach number M_c less than 2.0

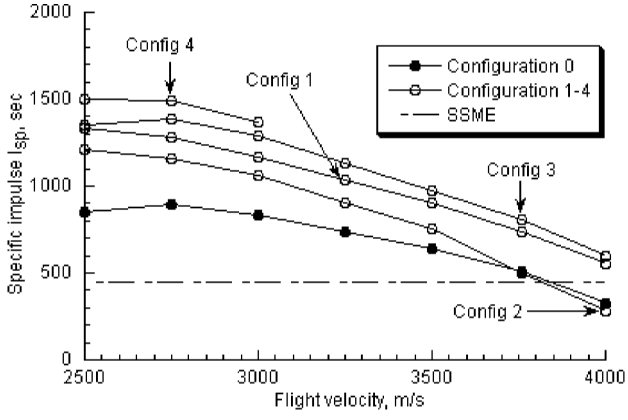

c) Combustor entrance Mach number M_c less than 2.5

Fig. 6 Comparison of best, viscous specific impulse.

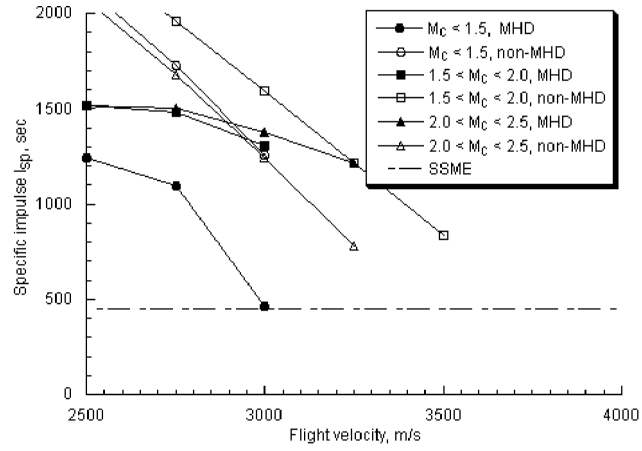

a) Configuration 4

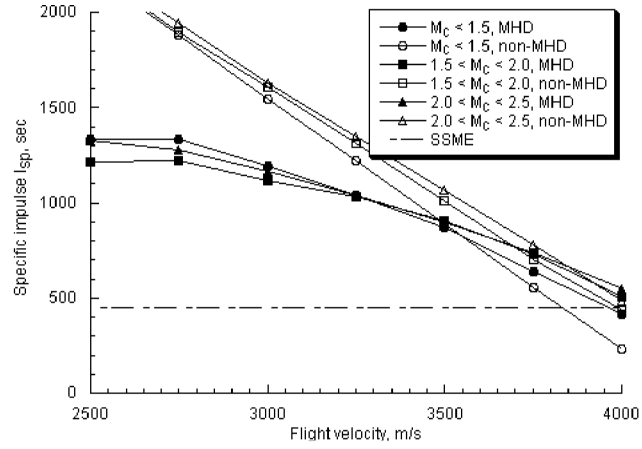

b) Configuration 1

Fig. 7 Comparison of best viscous specific impulses between MHD and non-MHD schemes.

In Fig. 7a, specific impulse values are compared for configuration 4 between the MHD and non-MHD cases. As mentioned in "Assumptions and Parameters," the length of the first ramp is held the same between the MHD and non-MHD designs. Because the ramp angle is higher for the non-MHD case, the air mass captured in the non-MHD vehicle is higher than that for the MHD vehicle. Under this constraint, Fig. 7a shows that the non-MHD cases result in higher specific impulse values, except for $2 < M_c < 2.5$, at high flight speeds.

In Fig. 7b, a similar comparison is made for configuration 1. Here again, the MHD values are generally lower than the non-MHD values. Only for flight speeds equal to or greater than 3750 m/s is the MHD value greater than the non-MHD value. For $M_c < 1.5$ and at the flight speed of 4000 m/s, the MHD case is better than the non-MHD case. However, the absolute value of specific impulse is no better than that of the SSME there.

Typical Operating Condition

The foregoing results lead to the conclusion that the nonequilibrium MHD scheme is generally no better than the non-MHD scheme. The overall best scheme is configuration 1. At $V = 3750$ m/s, $\theta = 18.9$ deg and $M_c < 1.5$, the MHD scheme has a substantial advantage, $I_{sp} = 646$ s as compared to $I_{sp} = 556$ s for the non-MHD scheme. The results for this case are listed in Tables 1–4, and the overall performance is presented in Table 5. In this case the lengths of the generator, the combustor, and the accelerator are 2.681, 0.464, and 2.772 m, respectively.

Table 1 Compression stages

Parameter	Freestream	First shock	Second shock	Third shock	Fourth shock
Pressure, Pa	1.039×10^3	2.846×10^4	1.494×10^5	4.326×10^5	1.000×10^6
Temperature, K	250	1485	2371	3265	3683
Density, kg/m^3	1.44×10^{-2}	6.65×10^{-2}	2.18×10^{-1}	4.49×10^{-1}	9.04×10^{-1}
Velocity, m/s	3750	3427	3062	2176	1687
Mach number	11.8	4.616	3.337	2.049	1.481

Table 2 Entrance of MHD devices and combustor

Parameter	Generator	Combustor	Accelerator
Channel height,[a] m	0.6027	0.7918	0.8373
Pressure, Pa	1.508×10^5	1.000×10^6	1.426×10^6
Temperature, K	2383	3683	3742
Velocity, m/s	3050	1687	1446
Mach number	3.107[a]	1.481	1.116
Conductivity, mho/m	39.1	NA	71.6
Magnetic field, T	4.50	NA	7.53
Hall parameter	7.68	NA	1.22
Axial voltage gradient, V/m	5263	NA	700
Transverse voltage gradient, V/m	13,030	NA	9610
Current density, A/m^2	2.668×10^4	NA	4.106×10^4
Voltage, V	7851	NA	9599
Impulsive external power, W	4.29×10^7	NA	NA
External power density q, W/m^3	3.55×10^9	NA	NA
Equilibration distance x_{eq}, m	0.091	NA	NA

[a]Frozen-flow value.

Table 3 Exit of MHD devices and combustor

Parameter	Generator	Combustor	Accelerator
Channel height,[a] m	0.7901	0.8358	0.6473
Pressure, Pa	1.581×10^5	1.426×10^6	1.371×10^6
Temperature, K	2770	3742	3736
Velocity, m/s	2597	1446	2105
Mach number	2.66	1.12	1.63
Conductivity, mho/m	39.1	NA	72.6
Magnetic field, T	4.50	NA	7.53
Hall parameter	7.40	NA	1.27
Axial voltage gradient, V/m	4321	NA	1058
Transverse voltage gradient, V/m	11,090	NA	13,900
Current density, A/m^2	3.944×10^4	NA	6.007×10^4
Voltage, V	8763	NA	8353
External power, W	0	NA	NA

[a]This dimension is for one flow path per 2.347 m of vehicle width.

The pressure amd temperature in the combustion chamber are 1×10^6 Pa and 3683 K, respectively, which are of similar magnitudes as in the equilibrium schemes.[2,3] However, unlike in the equilibrium schemes,[3] the required magnetic field strengths are only 4.50 and 7.53 T for the generator and accelerator, respectively, which can be achieved with the present-day technology.

The external power required, 273 MW per each meter of the vehicle width, is 19.3% of the fuel power generated in the combustor and 56.1% of the output from the generator. This power level is much higher than envisioned in the original nonequilibrium ionization concept.[4] The technology necessary for providing an external power of this magnitude to the vibron mode with a high efficiency is presently nonexistent.

Variations

The effect of varying the flight dynamic pressure on specific impulse is shown in Fig. 8 for the optimum condition. Fig. 8 shows that specific impulse improves with increasing dynamic pressure. However, the advantage of the MHD decreases with increasing dynamic pressure. The MHD scheme produces a significantly higher specific impulse than SSME at all flight dynamic pressures considered.

Table 4 Nozzle flow properties

Parameter	Starting	Ending
Channel height, m	0.2108[a]	7.45
Pressure, Pa	1.370×10^6	1.112×10^4
Temperature, K	3736	2164
Velocity, m/s	2105	3840
Frozen Mach number	1.54	3.91
O	3.256×10^{-2}	5.289×10^{-3}
N	1.268×10^{-3}	4.632×10^{-6}
H	7.900×10^{-2}	2.061×10^{-2}
Cs	3.410×10^{-4}	5.002×10^{-4}
O_2	1.965×10^{-2}	1.355×10^{-2}
N_2	5.503×10^{-1}	6.161×10^{-1}
H_2	8.996×10^{-2}	4.471×10^{-2}
NO	2.573×10^{-2}	1.462×10^{-2}
OH	6.380×10^{-2}	1.601×10^{-2}
H_2O	1.382×10^{-1}	2.686×10^{-1}
Cs^+	1.234×10^{-4}	1.380×10^{-5}

[a]This dimension is an equivalent one-dimensional value.

Table 5 Overall performance

Parameter	Value
Ramp angle, deg	18.9
Vehicle height, m	7.45
Air mass flow rate, kg/s	402.63
Fuel mass flow rate, kg/s	11.8
Seed mass flow rate, kg/s	1.21
Inlet area ratio	12.4
Nozzle area ratio	35.4
Momentum flow in, N	1.518×10^6
Momentum flow out (inviscid), N	1.679×10^6
Friction drag, N	6.462×10^4
Inviscid thrust, N	1.615×10^5
Inviscid thrust − friction drag, N	9.689×10^4
Electric power transferred, W	4.863×10^8
External power consumed, W	2.728×10^8
Inviscid specific impulse, s	1169
Viscous specific impulse, s	646
External/combustor power, η_1	0.193
External/generator output, η_2	0.561
Energy bypass ratio, η_3	0.168
Fuel-to-external power ratio assumed, η_4	1

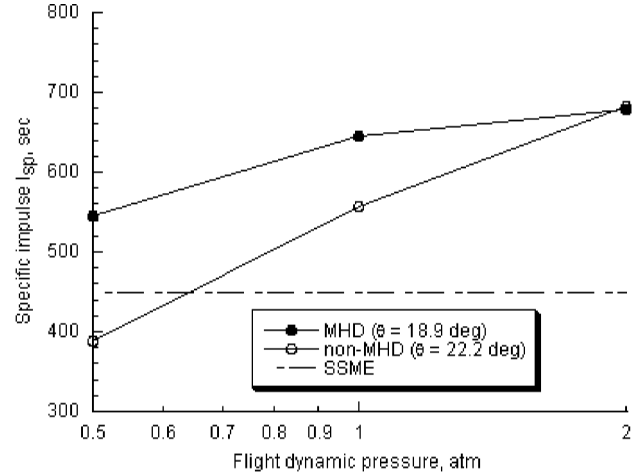

Fig. 8 Effect of flight dynamic pressure on best specific impulse: configuration 1, $V = 3750$ m/s, and M_c constrained at 1.5.

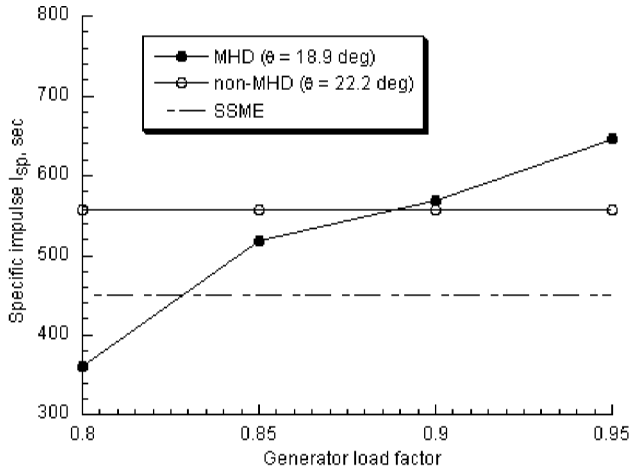

Fig. 9 Effect of load factor on best specific impulse: configuration 1, $V = 3750$ m/s, and M_c constrained at 1.5.

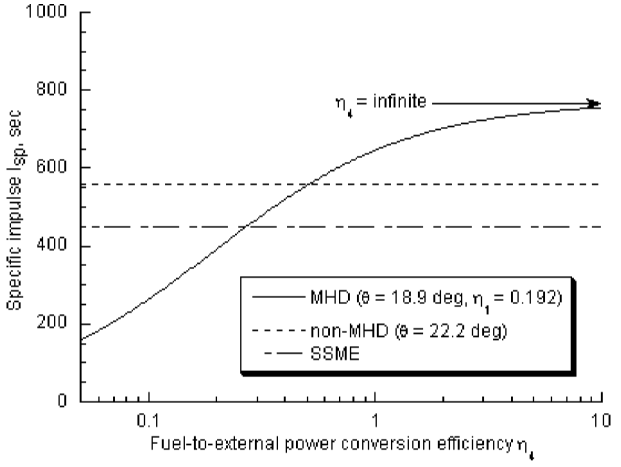

Fig. 10 Effect of the fuel-to-external power conversion efficiency η_4 on best specific impulse: configuration 1, $V = 3750$ m/s, and M_c constrained at best 1.5.

The effect of varying the load factor E_y/uB on specific impulse is shown in Fig. 9 for the same case. Figure 9 shows that the viscous specific impulse increases as the load factor approaches unity. This is expected: As the load factor approaches unity, there is less and less "slip" between the flow and the field driving the flow. Therefore, the energy loss, or entropy increase, becomes smaller. Note that the strengths of the applied field become larger as the load factor approaches unity. At load factors below 0.89, the MHD system produces specific impulses smaller than the non-MHD system.

The effect of varying the fuel-to-external power conversion efficiency η_4 on specific impulse is shown in Fig. 10 for the same case. These values are obtained with Eq. (10). When the η_4 value is lower than 0.1, specific impulse varies approximately linearly with η_4. The η_4 values greater than unity, shown in Fig. 10, represent the case where the external power is drawn partly or wholly from a nuclear power source. As shown, specific impulse improves significantly if external power can be obtained without using fuel. Conversely, if the energy conversion efficiency is poor, the specific impulse will be low.

In Fig. 11, comparison is made between the present nonequilibrium MHD scheme and the equilibrium MHD scheme presented in Ref. 3. The two best-performing configurations, configurfation 4 at flight speeds below 3000 m/s and configuration 1 for higher speeds, are selected for this comparison. The equilibrium MHD values are calculated with the method presented in Ref. 3, but by the use of the same constraints on the combustor area ratio as for the nonequilibrium case. They are, in the definition of the present work, for

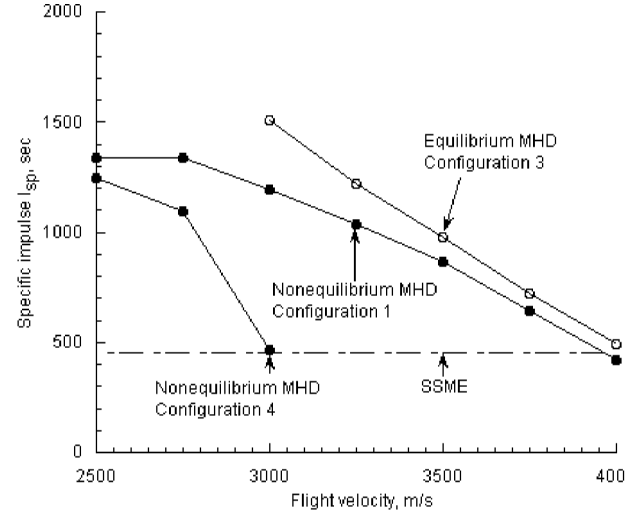

Fig. 11 Comparison between the best-performing nonequilibrium and equilibrium MHD schemes with M_c constrained at 1.5.

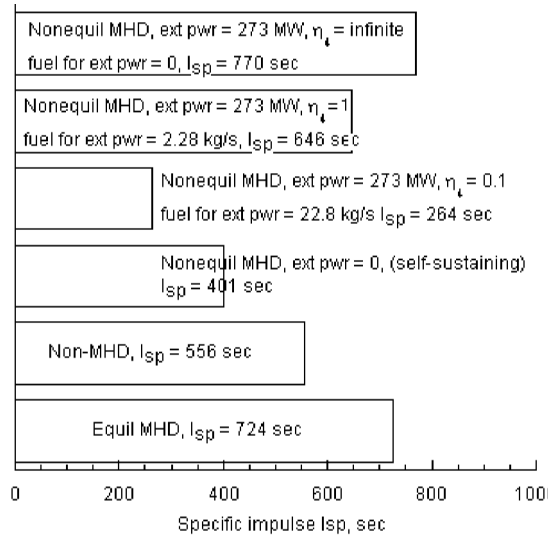

Fig. 12 Comparison of highest attainable specific impulse at $V = 3750$ m/s and $\theta = 18.9$ deg for configuration 1 with nonequilibrium MHD and $\theta = 17.1$ deg for configuration 3 with equilibrium MHD.

configuration 3. The two minor errors mentioned in the Introduction were also corrected in the equilibrium MHD calculation. The nonequilibrium MHD calculation for configuration 4 was stopped at $V = 3000$ m/s because the postshock temperature became so high that the nonequilibrium scheme was not necessary. Figure 11 illustrates that the thrust performance of the nonequilibrium MHD scheme can not exceed that of the equilibrium scheme.

Finally, in Fig. 12, the highest attainable specific impulse values are compared for the optimum condition among 1) the non-MHD, 2) the present MHD scheme with three different η_4 values, 3) the present MHD scheme in which the external ionizing power is drawn from the generator output, and 4) the equilibrium MHD scheme. As seen here, the present nonequilibrium scheme produces a higher specific impulse than the non-MHD case if η_4 is nearly unity or higher. However, the specific impulse of the nonequilibrium scheme is lower than that for the equilibrium scheme if η_4 is 1. For the self-sustaining case where the external power is drawn from the output of the generator, the specific impulse is calculated to be 401 s.

Discussion

The foregoing results contain two minor inaccuracies and one point of caution. The first inaccuracy is on the enthalpy of the flow.

As mentioned in "Ionization Schemes," the equilibrium flow calculation was made in the present work with the JANNAF coefficient, which is known to be inaccurate at low temperatures. This inaccuracy introduces a small inaccuracy in the equilibrium flow conditions over the first ramp. This inaccuracy remains throughout the flowpath because energy flow is conserved thereafter. This inaccuracy is tolerated here because the same inaccuracy exists for both the MHD and non-MHD cases, and, therefore, the relative merit of the MHD scheme is unaffected.

Secondly, there exist small inconsistencies in the cross-sectional areas because of normalization. Inside each component, a small inaccuracy accumulates along the flow because of numerical truncation. At the exit of each component, the cross-sectional area of the flowpath is reevaluated to conserve mass and energy, that is, normalized. This procedure produced a small but abrupt change in the cross-sectional area at the juncture points.

Additionally, one is cautioned that the sound speed is evaluated under the assumption of equilibrium in the equilibrium region, as well as the assumption of a frozen flow in the nonequilibrium region. This changing of the definition of sound speed appears as a sudden jump in Mach number at those juncture points.

As stated in Refs. 2, 3, and 12, research and technology developments are required toward making the MHD energy bypass propulsion concept a reality. These references have identified issues such as nonequilibrium ionization vs equilibrium ionization, acceleration of flow with Lorentz forces with minimum Joule heating, various losses in MHD devices, efficient and effective seeding for ionization, and a need for lightweight MHD devices for use on spaceplanes. Herein, we have addressed the issue of nonequilibrium ionization.

The calculation results presented show first that the external power required for achieving the degree of nonequilibrium ionization necessary for meaningful MHD action is a substantial fraction of the total enthalpy of the airflow (Fig. 4). This is because of the strong coupling between the ionization phenomenon and vibrational excitation phenomenon: external energy is expended mostly to raise the vibrational temperature of air molecules and to maintain it against the collisional cooling by the cold airflow. The external power required is of the same order as the power output from the generator (Fig. 5a).

The nonequilibrium ionization scheme was proposed for efficient operation at low ramp angles.[4] However, at low ramp angles, the propulsion system produces only a relatively small momentum increase. The turbulent skin friction, which is a relatively weak function of flow properties, is a relatively large portion of the total drag at low ramp angles. As a result, the specific impulse is low at low ramp angles.

The simplified analysis presented herein suggests that the load factor of the MHD devices must be higher than 0.83 for the nonequilibrium MHD scheme to be superior to the SSME, if the flight speed is 3750 m/s and if the combustor inlet Mach number is limited to 1.5. The assumed uniform ionization will require uniform distribution of cesium. Because of the large Hall parameters, it may be beneficial to use a diagonally connected electrode arrangement[13] rather than Faraday electrode connections. The high Hall parameter does also raise concerns about the possibility of instabilities.

At the ramp angles where the MHD system begins to be comparable to or better than the non-MHD system, the flow reaches equilibrium within a short distance from the entrance. Most of the MHD action occurs in the equilibrium region. A relatively large external power must be delivered to the flow in the small nonequilibrium region. Based on the quasi-one-dimensional analysis, the equilibrium scheme[3] is superior in performance to the nonequilibrium scheme. The benefit of the nonequilibrium MHD scheme exists only when the external power can be produced by converting fuel energy very efficiently, or by not expending fuel at all.

Conclusions

In an MHD-energy bypass scramjet system that uses external power to produce electrically conductive flow, the external power is expended mostly to heat the vibrational mode of air molecules. The nonequilibrium region is small, and most of the MHD action occurs in the equilibrium region. The external power needed, partly for initiating the nonequilibrium ionized flow and partly for maintaining it, is of the same order as the power generated in the MHD generator and is a significant fraction of the power derived from the fuel in the combustor. The specific impulse depends on the efficiency of conversion of the fuel energy to the external power and the load factor. The highest attainable specific impulse is slightly higher than that of the conventional non-MHD scramjet, if the external ionizing power can be obtained by an efficient means, but it is lower than that of an MHD system relying entirely on equilibrium ionization. An MHD energy bypass propulsion scheme looks to be more promising with the equilibrium ionization scheme than with the nonequilibrium scheme.

Acknowledgment

The first two authors wish to acknowledge the support provided by NASA Ames Research Center through Contract NAS2-99092 to ELORET Corporation.

References

[1]Bityurin, V. A., Lineberry, J. T., Potebnia, V. G., Alferov, V. I., Kuranov, A. L., and Sheikin, E. G., "Assessment of Hypersonic MHD Concepts," AIAA Paper 97-2393, June 1997.

[2]Park, C., Bogdanoff, D. W., and Mehta, U. B., "Theoretical Performance of Frictionless MHD-Bypass Scramjet," *Journal of Propulsion and Power*, Vol. 17, No. 3, 2001, pp. 591–598.

[3]Park, C., Mehta, U. B., and Bogdanoff, D. W., "MHD Energy Bypass Scramjet Performance with Real Gas Effects," *Journal of Propulsion and Power*, Vol. 17, No. 5, 2001, pp. 1049–1057.

[4]Macheret, S., "Electron Beam Generated Plasmas in Hypersonic MHD Channels," AIAA Paper 99-3635, June 1999.

[5]Park, C., Mehta, U. B., and Bogdanoff, D. W., "Theoretical Performance of a MHD-Bypass Scramjet with Nonequilibrium Ionization," NASA TM-2001-210918, June 2001.

[6]Park, C., *Nonequilibrium Hypersonic Aerothermodynamics*, Wiley, New York, 1990, Chap. 4, pp. 119–143; Chap. 2, pp. 43–88; and Chap. 8, pp. 255–269.

[7]Bruno, C., and Rosa-Clot, M., "Hybrid Alpha Thruster for Attitude Control," International Astronautical Federation, Paper IAF-96-S.4.02, Oct. 1996.

[8]Perini, L. L., "Curve Fit of JANAF Thermochemical Data," Rept. ANSP-M-5, Johns Hopkins Univ., Applied Physics Lab., Baltimore, MD, Sept. 1972.

[9]McBride, B. J., and Gordon, S., "Computer Program for Calculation of Complex Chemical Equilibrium Compositions and Applications," NASA-RP-1311, 1996.

[10]Bourdon, A., and Vervisch, P., "Analytical Models for Electron–Vibration Coupling in Nitrogen Plasma Flows," *Journal of Thermophysics and Heat Transfer*, Vol. 14, No. 4, 2000, pp. 489–495.

[11]Van Driest, E. R., "Turbulent Boundary Layer in Compressible Flow," *Journal of the Aeronautical Sciences*, Vol. 18, No. 3, 1951, pp. 145–160.

[12]Chase, R. L., Mehta, U. B., Bogdanoff, D. W., Park, C., Lawrence, S. L., Aftosmis, M. J., Macheret, S., and Shneider, M., "Comments on an MHD Energy Bypass Engine Powered Spaceliner," AIAA Paper 1999-4975, Nov. 1999.

[13]Rosa, R. J., *Magnetohydrodynamic Energy Conversion*, McGraw–Hill, New York, 1968, pp. 64–66.